Nonlinear Dyn (2020) 99:1893–1908
https://doi.org/10.1007/s11071-019-05424-5

ORIGINAL PAPER

Normal modes of a double pendulum at low energy levels

Ivana Kovacic · **Miodrag Zukovic** · **Dragi Radomirovic**

Received: 1 May 2019 / Accepted: 9 December 2019 / Published online: 3 January 2020

Abstract This study is concerned with a double pendulum and its regular behaviour associated with low energy levels and the influence of the associated initial conditions on the frequency of normal modes. The case of nonlinear oscillations described by the exact equations of motion is examined. A global qualitative insight is provided via energy diagrams and Poincaré maps. Then, the case of linear oscillations, their normal modes and associated frequencies is analysed. Further, quantitative insights via two approaches (Lindstedt–Poincaré method and harmonic balancing) are also achieved to determine analytically the influence of initial amplitudes on the existence and frequency of nonlinear normal modes. These results are compared with the one corresponding to the linear normal modes as well as with the corresponding numerical solutions of the exact equations of motion.

Keywords Double pendulum · Normal modes · Linear system · Nonlinear system · Low energy level

1 Introduction

A classical pendulum is one of the paradigms of vibration theory, as its behaviour is associated with rich and interesting dynamic behaviour. One can distinguish a simple or physical pendulum. A simple (mathematical) pendulum consists of a point mass m attached to a hinged weightless rod of length m or a mass suspended by a weightless non-deformable string/rope. A physical pendulum consists of a rigid body that is pivoted at a certain point, and one of its realization is a uniform massive rod of length l and mass m pivoted at one end. Pendula that move in a vertical plane are characterized by two equilibria: lower (stable) and upper (unstable). For small deviations from the lower equilibrium, these oscillations are harmonic and can be described by sine or cosine functions. Its period is constant—it does not depend on the initial conditions, i.e. on the energy level E, but it does depend on the system natural frequency ω_n. (In case of the simple pendulum, this parameter is $\omega_n^2 = g/l$, while in the case of the uniform massive rod, it corresponds to $\omega_n^2 = 1.5g/l$). As the energy level increases but stays in the domain $-\omega_n^2 < E < \omega_n^2$, the periodicity of the resulting motion still holds. As the amplitude becomes larger, the influence of geometric nonlinearity is brought to bear and the period becomes amplitude-dependent. The exact

Electronic supplementary material The online version of this article (https://doi.org/10.1007/s11071-019-05424-5) contains supplementary material, which is available to authorized users.

I. Kovacic (✉) · M. Zukovic
Centre for Vibro-Acoustic Systems and Signal Processing, Faculty of Technical Sciences, University of Novi Sad, Novi Sad, Serbia
e-mail: ivanakov@uns.ac.rs

D. Radomirovic
Faculty of Agriculture, University of Novi Sad, Novi Sad, Serbia

value of the period can be expressed in terms of the elliptic integral of the first kind [1]. Note, however, that if the simple pendulum wraps around a cycloid, even its large-amplitude oscillations are characterized by the period that is amplitude-independent [2]. Going back to classical pendula and the influence of energy levels on its behaviour, it is known that for $E > \omega_n^2$, rotating/spinning motion around the hinge occurs.

A double pendulum, which consists of two simple pendula or two compound/physical pendula, behaves quite differently, involving regular and chaotic motion associated with a torus, which becomes deformed and decays. In the regime of small oscillations, the double pendulum exhibits coupled harmonic oscillations, which are linear combinations of normal modes. The resulting motion can be periodic or quasi-periodic, and this depends on the fact whether two associated angular frequencies are commensurable or not. As the energy level increases, the oscillations become chaotic. Given the fact that the double pendulum is a Hamiltonian system, the KAM theorem [3] holds, stating that if this system is subjected to a weak nonlinear perturbation, some of the invariant tori that have 'sufficiently irrational' frequencies survive, implying further existence of some quasi-periodic motion. Motivated by the fact that Hamiltonian textbook systems, such as the double pendulum, had been seen as simple, Richter and Scholz [4] used numerical approach via Poincaré sections to demonstrate the bewildering complexity of the dynamic behaviour that this simple system exhibits. Shinbrot et al. [5] used a Polaroid® camera to photograph the stroboscopic trajectory of the double pendulum, measuring experimentally the exponential rate of separation of nearby trajectories, which is characteristic of chaotic systems. They demonstrated good agreement between their experiments and numerical simulations, calculating also the positive Lyapunov exponent, as expected for a chaotic system. Levien and Tan [6] used optical encoder wheels to catch experimentally and quantify sensitive dependence on initial conditions, the signature of chaos, in a double pendulum system. Stachowiak and Okada [7] provided further numerical results concerning the planar double pendulum system, exploring chaotic features of its behaviour via Poincaré' sections, bifurcation diagrams and Lyapunov exponents. A bifurcation parameter in their bifurcation diagrams that which illustrate transformations from regular behaviour into globally chaotic motion is energy. Rafat et al. [8] investigated a variation of the simple double pendulum in which the two particles are replaced by square plates. As such, this system represents a compound pendulum, but the centre of mass of the inner plate does not lie along the line joining the two hinges. The authors showed that the onset of chaos occurs at a significantly lower energy than for the simple double pendulum. Unlike these studies, Jyotirmoy et al. [9] pointed out the shortage of investigations of the regular behaviour of a double simple pendulum at lower energy region. They applied approximate analytical techniques and provided numerical confirmations to demonstrate the influence of initial conditions on normal modes. The following study is aimed at providing deeper insights into such behaviour, focusing on a double compound pendulum consisting of two unequal or equal rods at low energy levels and detecting the initial conditions for which linear and nonlinear normal modes exist. To that end, numerical solutions are used, and two approximate analytical techniques are adjusted to determine these initial conditions and the resulting vibration frequencies.

2 Model and its global behaviour

2.1 Mechanical and mathematical model

The system considered herein has the form of a planar double compound pendulum hinged at Point O, encompassing two uniform massive rods OA and AB (Fig. 1a) that may be of unequal masses (m_1, m_2) and lengths (l_1, l_2), or, in a special case analysed later on, of equal mass m and length l. The generalized coordinates are taken to be the angles between each rod and the vertical: φ and ψ (Fig. 1a). The centres of masses of each rod are labelled by C_1 and C_2.

As the first rod OA performs rotation about the fixed axis and the second rod AB is in plane motion, the overall kinetic energy is given by:

$$T = \frac{1}{2}\left(\frac{m_1}{3} + m_2\right) l_1^2 \dot{\varphi}^2 + \frac{1}{6} m_2 l_2^2 \dot{\psi}^2 + \frac{1}{2} m_2 l_2 l_1 \dot{\varphi}\dot{\psi} \cos(\varphi - \psi). \quad (1)$$

Using the position of the centres of masses noted in Fig. 1b, the gravitational potential energy can be written down in the following form:

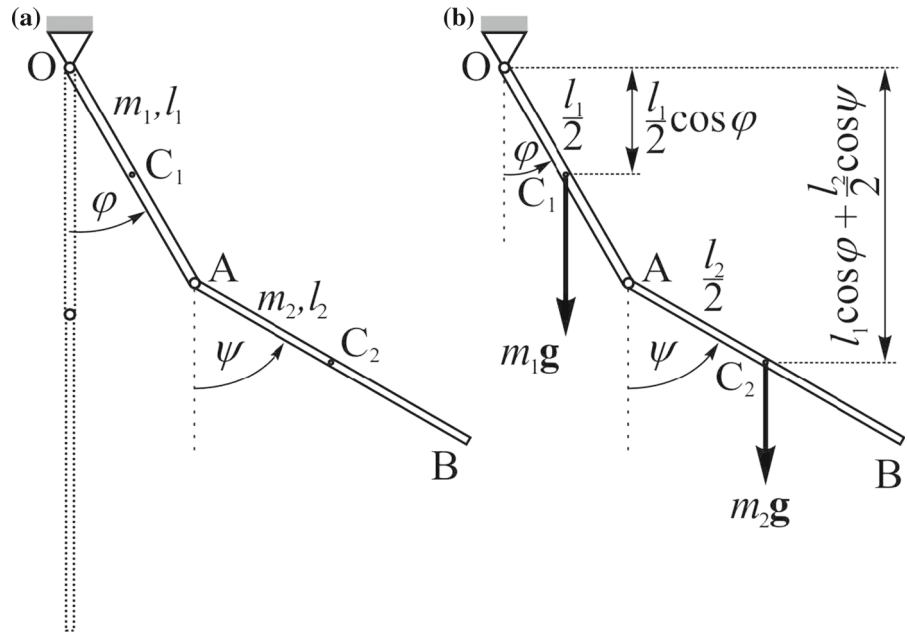

Fig. 1 **a** Double pendulum under consideration; **b** gravitational forces and the coordinates of the centres of masses

$$V = -\frac{1}{2}g(l_1(m_1 + 2m_2)\cos(\varphi) + l_2 m_2 \cos(\psi)). \quad (2)$$

Based on Lagrange's equation of the second kind $\frac{\mathrm{d}}{\mathrm{d}t}\frac{\partial T}{\partial \dot{q}} - \frac{\partial T}{\partial q} = -\frac{\partial V}{\partial q}, q \in \{\varphi, \psi\}$, the system of following equations of motion is derived:

$$\left(\frac{m_1}{3} + m_2\right) l_1^2 \ddot{\varphi} + \frac{m_2 l_1 l_2}{2}\cos(\varphi - \psi)\,\ddot{\psi} + \frac{m_2 l_1 l_2}{2}\sin(\varphi - \psi)\,\dot{\psi}^2 + \frac{(m_1 + 2m_2)\,g l_1}{2}\sin\varphi = 0, \quad (3)$$

$$\frac{m_2 l_1 l_2}{2}\cos(\varphi - \psi)\,\ddot{\varphi} + \frac{m_2 l_2^2}{3}\ddot{\psi} - \frac{m_2 l_1 l_2}{2}\dot{\varphi}^2 \sin(\varphi - \psi) + \frac{m_2 g l_2}{2}\sin\psi = 0. \quad (4)$$

These equations are coupled and nonlinear both with respect to the generalized coordinates and the generalized velocities.

By introducing a set of the following parameters (a non-dimensional mass ratio, a non-dimensional length ratio, a non-dimensional time and the square of the natural frequency ω_n^2):

$$\mu = \frac{m_2}{m_1}, \quad \lambda = \frac{l_2}{l_1}, \quad \tau = \omega_n t, \quad \omega_n^2 = \frac{g}{l_1}, \quad (5)$$

the equations of motion can be presented in the following non-dimensional form:

$$(6\mu + 2)\,\ddot{\varphi} + 3\lambda\mu\cos(\varphi - \psi)\,\ddot{\psi} + 3\lambda\mu\sin(\varphi - \psi)\,\dot{\psi}^2 + (6\mu + 3)\sin(\varphi) = 0, \quad (6)$$

$$3\cos(\varphi - \psi)\,\ddot{\varphi} + 2\lambda\ddot{\psi} - 3\sin(\varphi - \psi)\,\dot{\varphi}^2 + 3\sin\psi = 0. \quad (7)$$

2.2 Energy considerations

To get a global insight into the behaviour of this system described by Eqs. (1) and (2) at lower energy levels, two non-dimensional energy parameters are introduced: $E = \frac{T+V}{m_1 g l_1}$, $E_0 = \frac{T_0+V_0}{m_1 g l_1}$. The energy level that corresponds to the zero value of the kinetic energy, i.e. to the positions $\dot{\varphi}(0) = \dot{\psi}(0) = 0$ when the pendula change the direction of motion, is given by:

$$E = E_0 = \frac{V_0}{m_1 g l_1} = -\frac{1}{2}(\lambda\mu\cos(\psi_0) + (2\mu + 1)\cos(\varphi_0)). \quad (8)$$

Note that the subsequent analysis regards the region in which the generalized coordinates take equal values, or the values located between $-\pi$ and π.

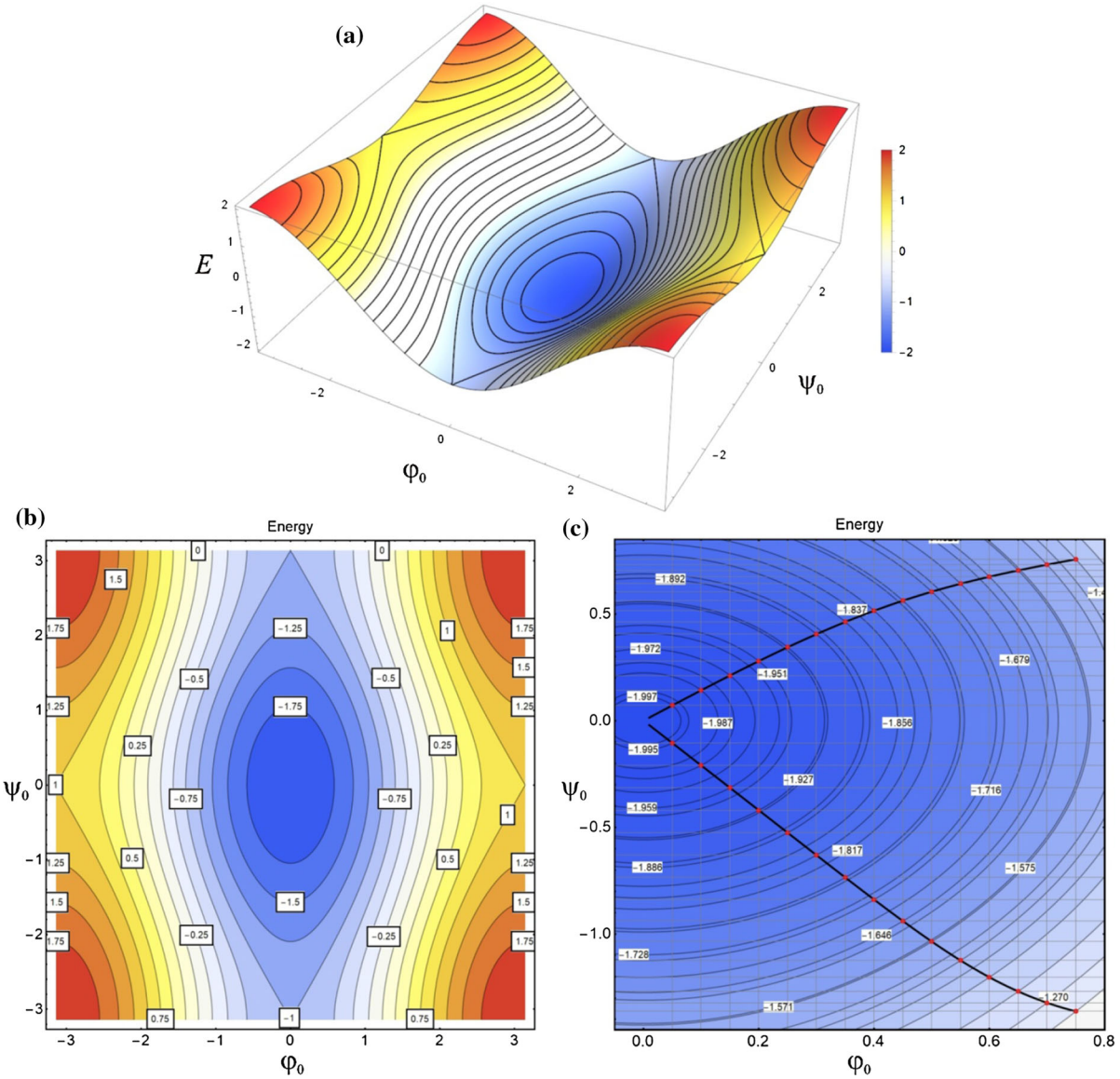

Fig. 2 **a** Surface $\varphi_0 - \psi_0 - E$ corresponds to the case of equal pendula $\mu = 1, \lambda = 1$; **b** projections of the surface from **a** onto the $\varphi_0 - \psi_0$ plane; **c** enlarged version of the part of the blue region from **b** for $-2 < E < -1$

Two vertical continuous configurations $\varphi(0) = \psi(0) = 0$ and $\varphi(0) = \psi(0) = \pi$ are associated, respectively, with the following values of the energy minimum and maximum:

$$E_{min} = -\frac{1}{2}(\lambda\mu + (2\mu + 1)), \tag{9}$$

$$E_{max} = \frac{1}{2}(\lambda\mu + (2\mu + 1)). \tag{10}$$

Two vertical discontinuous configurations $\varphi(0) = 0, \psi(0) = \pi$ and $\varphi(0) = \pi, \psi(0) = 0$ are associated respectively with two energy levels at which separatrices occur:

$$E_{sep} = -\frac{1}{2}(-\lambda\mu + (2\mu + 1)), \tag{11}$$

$$E_s = -\frac{1}{2}(\lambda\mu - (2\mu + 1)). \tag{12}$$

The energy levels defined by Eqs. (8)–(12) are used to plot the surface $\varphi_0 - \psi_0 - E$ that corresponds to the case of equal pendula $\mu = 1, \lambda = 1$ (Fig. 2a). Centres and saddles are clearly visible as well as periodic orbits

surrounding centres, separatrices connecting saddles and trajectories between the separatrices corresponding to spinning. The projections of this surface onto the $\varphi_0 - \psi_0$ plane with the energy levels are calculated from Eqs. (8)–(12) and noted in boxes in Fig. 2b. In this case, the energy levels (9) and (10) are equal, respectively, to -2 and 2 and correspond to the centres, while the energy levels (11) and (12) are equal, respectively, to -1 and 1 and correspond to the separatrices through saddles. Of interest for this work is the regular periodic motion that lies in the blue region around the centre (0,0). The enlarged version of this motion, which is obtained for $-2 < E < -1$, is shown in Fig. 2c. Note that this figure also contains a black solid line and red circles that will be commented on in the penultimate section of this article.

In order to gain a deeper insight into global behaviour at low energy levels, Poincaré maps are obtained for zero initial angular velocities. The value of ψ_0 and the initial energy are fixed, while φ_0 is calculated from the energy conservation law. Numerical integration is then carried out with these initial conditions, and the values of ψ and $\dot{\psi}$ for which $\dot{\varphi} = 0$ from the positive side are mapped. Figure 3 shows the Poincaré maps created for different energy values indicated above each map for two identical physical pendula ($\mu = 1, \lambda = 1$). When E=-1.9, two centres and surrounding closed orbits are seen, implying regular behaviour. As the energy level increases, the invariant tori become deformed. A saddle is seen when E=-1, where the trajectory passing through it is the envelope of the Poincaré map. The map plotted for $E = -0.8$ shows progressive motion with scattered points, which implies chaos. Animation 1 enclosed to this paper contains these Poincaré maps changing continuously for the increasing energy level. Animation 2, which is also enclosed to this paper, contains animated Poincaré maps corresponding to the case $\mu = 1, \lambda = 4/3$, illustrating qualitatively the same scenario with a quantitative difference with respect to the value of the energy.

3 Vibration in normal modes

3.1 Linear oscillations

When the system under consideration performs small (linear) oscillations, the equations of motion given by Eqs. (6) and (7) become:

$$(6\mu + 2)\,\ddot{\varphi} + 3\lambda\mu\,\ddot{\psi} + (6\mu + 3)\,\varphi = 0, \tag{13}$$

$$3\ddot{\varphi} + 2\lambda\ddot{\psi} + 3\psi = 0. \tag{14}$$

Assuming the solution for the response in the form $\varphi = A_1 \cos(\omega\tau)$, $\psi = A_2 \cos(\omega\tau)$ and deriving the characteristic equation [10], one can calculate two natural frequencies:

$$\omega_1 = \sqrt{3}\sqrt{\frac{1 + \lambda + 3\mu + 2\lambda\mu - \sqrt{(1+3\mu)^2 + (\lambda + 2\lambda\mu)^2 + \lambda\left(-2 - \mu + 6\mu^2\right)}}{\lambda\,(4 + 3\mu)}}, \tag{15a}$$

$$\omega_2 = \sqrt{3}\sqrt{\frac{1 + \lambda + 3\mu + 2\lambda\mu + \sqrt{(1+3\mu)^2 + (\lambda + 2\lambda\mu)^2 + \lambda\left(-2 - \mu + 6\mu^2\right)}}{\lambda\,(4 + 3\mu)}}, \tag{15b}$$

which are associated with two mode ratios

$$b_1 = \frac{A_2}{A_1} = \frac{-1 + \lambda - 3\mu + 2\lambda\mu + \sqrt{\lambda(1+2\mu)(-2+3\mu) + (1+3\mu)^2 + (\lambda+2\lambda\mu)^2}}{3\lambda\mu}, \tag{16a}$$

$$b_2 = \frac{A_2}{A_1} = \frac{-1 + \lambda - 3\mu + 2\lambda\mu - \sqrt{\lambda(1+2\mu)(-2+3\mu) + (1+3\mu)^2 + (\lambda+2\lambda\mu)^2}}{3\lambda\mu}. \tag{16b}$$

When two physical pendula are identical ($\mu = 1, \lambda = 1$), these two natural frequencies have the following values:

$$\omega_1 = \sqrt{\frac{3}{7}(7 - 2\sqrt{7})} = 0.85569, \tag{17a}$$

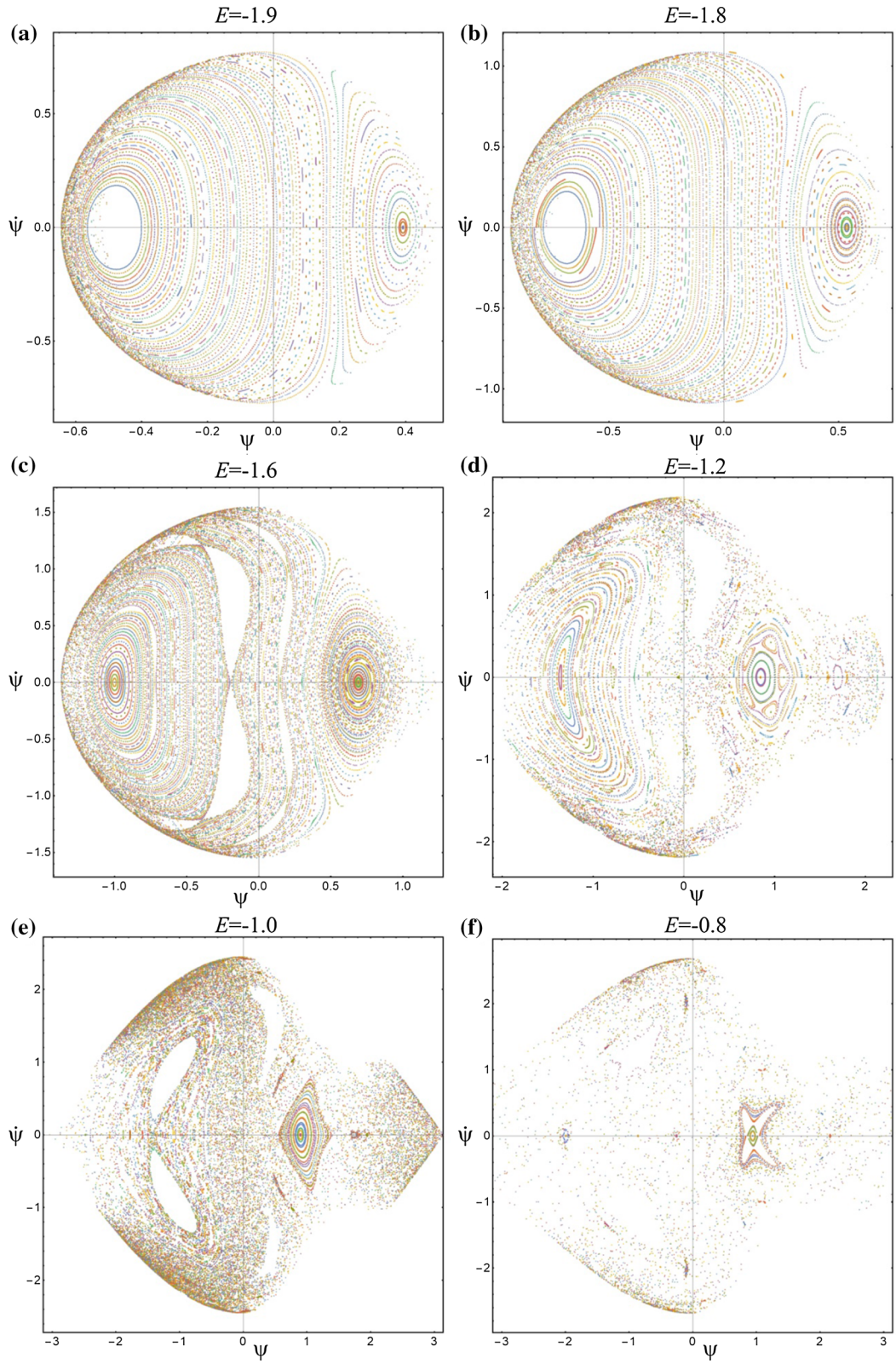

Fig. 3 Poincaré maps of two identical physical pendula ($\mu = 1, \lambda = 1$) for different energy values noted above each map

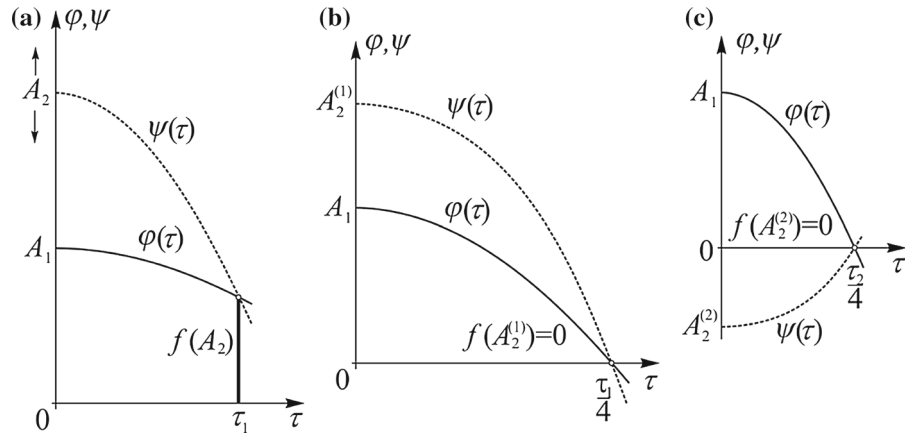

Fig. 4 **a** Intersection of the solutions for motion in a general case as a function of the initial amplitude $f = f(A_2)$; **b** case corresponding to NNM1, when the intersection is on the abscissa; **c** case corresponding to NNM2, when the intersection is on the abscissa

$$\omega_2 = \sqrt{\frac{3}{7}(7+2\sqrt{7})} = 2.29517, \tag{17b}$$

while the mode ratios have different values and the opposite sign:

$$b_1 = \frac{A_2}{A_1} = \frac{1}{3}\left(-1+2\sqrt{7}\right) = 1.43, \tag{18a}$$

$$b_2 = \frac{A_2}{A_1} = \frac{1}{3}\left(-1-2\sqrt{7}\right) = -2.1. \tag{18b}$$

Thus, in Mode 1, the pendula oscillate in-phase, while in Mode 2 they oscillate out-of-phase. The configurations that corresponds to Mode 1 and Mode 2 are shown in Fig. 3a. In a general case, the motion is a linear combination of these two normal modes.

Note that the mode ratios will have the same absolute values when $\mu = 1$, $\lambda = 4/3$, i.e. when the masses are the same, but the second pendulum is longer than the first one for 33%. The natural frequencies are then:

$$\omega_1 = \frac{3\sqrt{14}}{14} = 0.80178, \tag{19a}$$

$$\omega_2 = \frac{3\sqrt{2}}{2} = 2.1213, \tag{19b}$$

while the mode ratios are:

$$b_1 = \frac{A_2}{A_1} = 1.5, \tag{20a}$$

$$b_2 = \frac{A_2}{A_1} = -1.5. \tag{20b}$$

The configurations that correspond to these two modes: Mode 1 and Mode 2, are shown in Fig. 3b.

3.2 Nonlinear case

3.2.1 Exact solutions

The next task regards the double pendulum performing large-amplitude oscillations. The corresponding mathematical model is given by the exact equations of motion (6) and (7). Of interest here is to find numerically their solutions that have the properties of nonlinear normal modes (NNM) [11]: i) that they pass through their equilibrium position at the same time, and ii) that they vibrate at the same frequency. The initial conditions are assumed to be with nonzero initial amplitudes and with zero initial angular velocities, i.e. $\varphi(0) = A_1$, $\psi(0) = A_2$ $\dot{\varphi}(0) = 0$, $\dot{\psi}(0) = 0$.

In a general case, the solutions for φ and ψ do not pass simultaneously through zero values, i.e. their time histories intersect at a point that lies at a certain distance from the τ-axis. Let this distance be labelled by a function f. By fixing the value of A_1, one can treat this function as being depended on A_2: $f = f(A_2)$, as shown in Fig. 4a. An algorithm for detecting normal modes involves finding A_2 for the fixed A_1 while $f(A_2) = 0$. Positive values of A_2 (labelled by $A_2^{(1)}$ in Fig. 4b) will correspond to nonlinear normal Mode 1 (NNM1) analogous to Mode 1 in the linear case. Negative values of A_2 (labelled by $A_2^{(2)}$ in Fig. 4c) will correspond to nonlinear normal Mode 2 (NNM2) analogous to Mode 2 in the linear case. These NNM1 and NNM2 solutions are plotted in Fig. 5a as solid lines together with the solutions for the linear case, which are shown as green dotted lines. For smaller values of A_1, the solutions for the linear case are the tangents of the solutions corresponding to the nonlinear case.

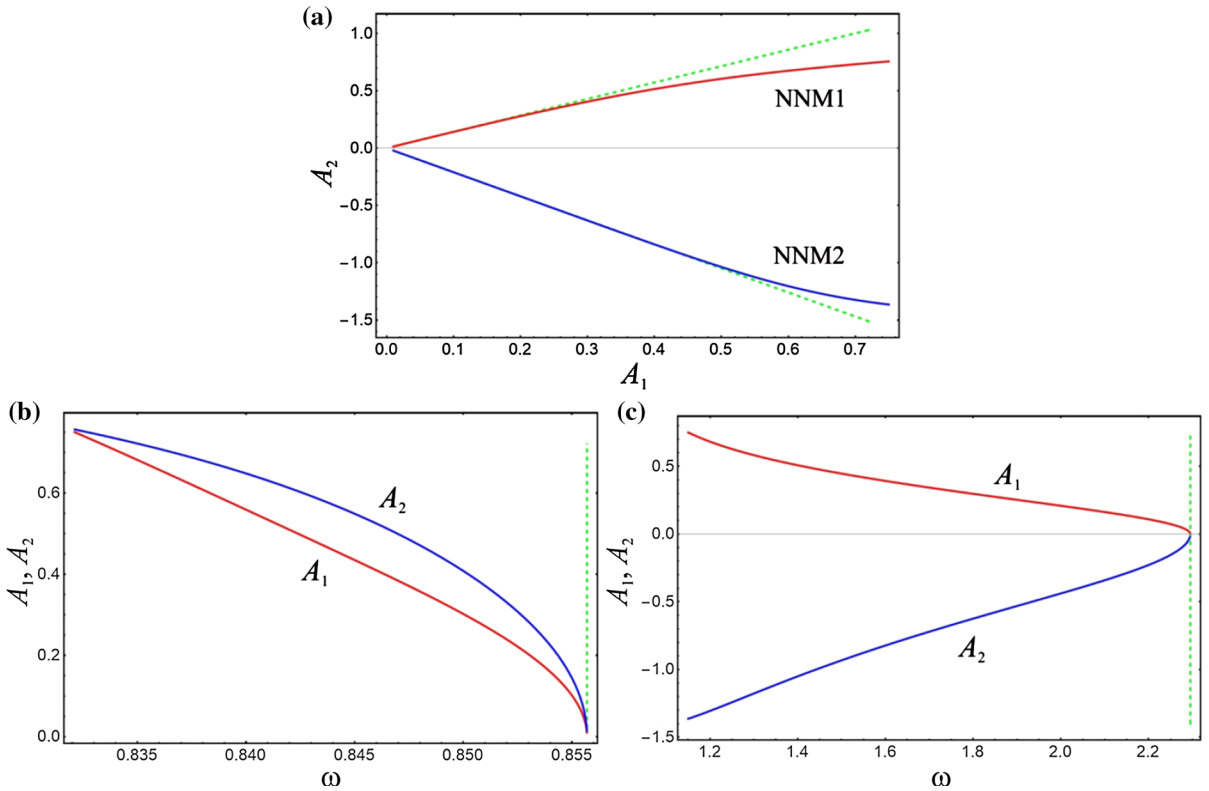

Fig. 5 Case of two identical physical pendula $\mu = 1, \lambda = 1$: **a** combinations of initial amplitudes yielding vibrations in normal modes; **b** influence of initial conditions on the in-phase mode; **c** influence of initial conditions on the frequency of the out-of-phase mode. Green dotes—solutions for the linear system; red solid line—solutions for A_1 in NNM1; and blue solid line—solutions for A_2 in NNM2. (Color figure online)

As the value of A_1 increases, the absolute values of A_2 decrease for both NNM1 and NNM2. Note that the solutions for Mode 2 and NNM2 coincide for larger values of A_1 than for Mode 1 and NNM1.

The moment of time when $f(A_2) = 0$ corresponds to the quarter of the period, and it can be used to calculate the frequency $\omega_1 = 2\pi/\tau_1$ (Fig. 4b) and $\omega_2 = 2\pi/\tau_2$ (Fig. 4c). These values are plotted in Fig. 5b and 6c for both NNMs of two identical pendula ($\mu = 1, \lambda = 1$), together with the solutions for the linear case given by Eqs. (18a, 18b). As the initial amplitudes increase (Fig. 5b), the frequency of NNM1 decreases from the value corresponding to the frequency of the linear Mode 1, Eq. (17a). By decreasing the absolute values of the initial amplitudes (Fig. 5c), the frequency of NNM2 increases until the value of the frequency of the linear Mode 2, Eq. (17b).

From a qualitative point of view, these diagrams have the same form for the case $\mu = 1, \lambda = 4/3$ (Fig. 6a–c), whose linear normal modes are shown in Fig. 7c, d. From a quantitative point of view, the difference is more apparent when comparing Fig. 6a with Fig. 5a: the values of the initial amplitudes for which the solutions for Mode 1 and NNM1 as well as the solutions for Mode 2 and NNM2 coincide are different.

3.2.2 *Approximate solutions by Lindstedt–Poincaré method*

By introducing the approximated expressions: $\sin\varphi \approx \varphi - \frac{\varphi^3}{6}$, $\sin\psi \approx \psi - \frac{\psi^3}{6}$, $\cos(\varphi - \psi) \approx 1 - \frac{(\varphi-\psi)^2}{2}$, $\sin(\varphi - \psi) \approx \varphi - \psi$, into the exact equations of motion given by Eqs. (6) and (7), the following approximated differential equations of motion are obtained:

$$(6\mu + 2)\ddot{\varphi} + 3\left(\lambda\mu\left(1 - \frac{1}{2}(\varphi - \psi)^2\right)\ddot{\psi}\right.$$
$$\left. + 3\lambda\mu\dot{\psi}^2(\varphi - \psi) + 2\mu\left(\varphi - \frac{\varphi^3}{6}\right)\right.$$

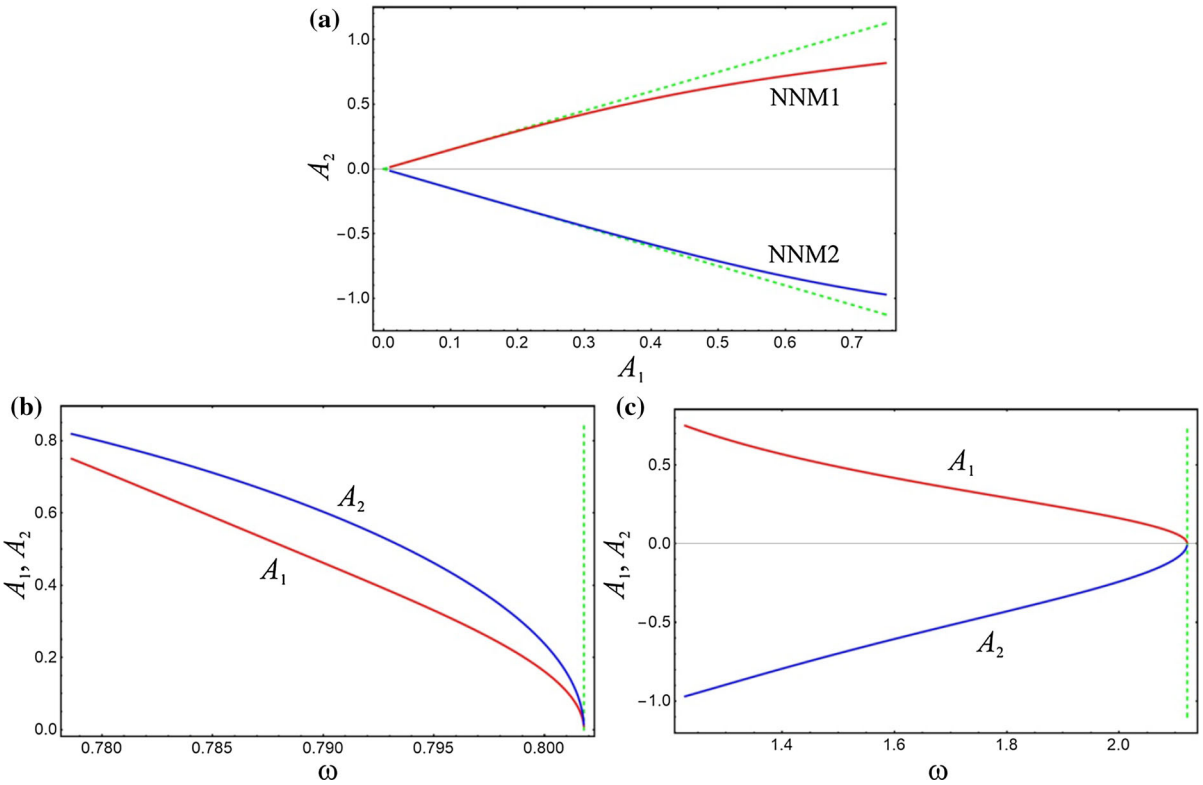

Fig. 6 Case $\mu = 1, \lambda = 4/3$: **a** combinations of initial amplitudes yielding vibrations in normal modes; **b** influence of initial conditions on the in-phase mode; **c** influence of initial conditions on the frequency of the out-of-phase mode. Green dotes—solutions for the linear system; red solid line—solutions for A_1 in NNM1; and blue solid line—solutions for A_2 in NNM2. (Color figure online)

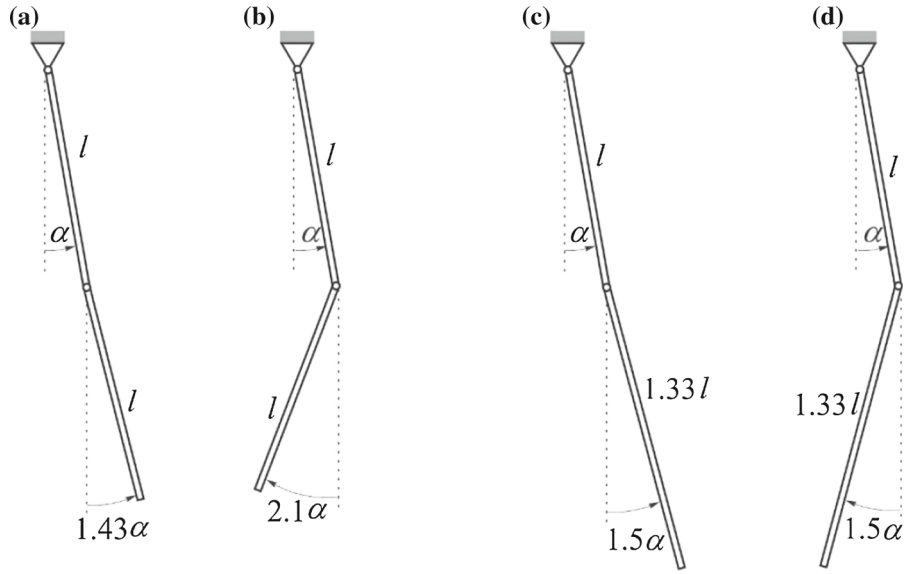

Fig. 7 **a**, **b** Mode shapes corresponding to the case of two identical physical pendula, $\mu = 1, \lambda = 1$; **c**, **d** mode shapes corresponding to the case $\mu = 1, \lambda = 4/3$

$$-\frac{\varphi^3}{6}+\varphi\Big)=0, \tag{21}$$

$$3\left(1-\frac{1}{2}(\varphi-\psi)^2\right)\ddot{\varphi}+2\lambda\ddot{\psi}$$
$$-3\dot{\varphi}^2(\varphi-\psi)+3\left(\psi-\frac{\psi^3}{6}\right)=0. \tag{22}$$

Their nonlinearity is cubic, which can be seen as suitable for the application of the Lindstedt–Poincaré method. However, one should first present these equations in the appropriate form of perturbed oscillators whose natural frequencies correspond to the natural ones obtained for linear oscillations in Sect. 3.1. For the sake of that, the following transformations to normal coordinates are introduced:

$$\varphi = X+Y, \tag{23a}$$
$$\psi = b_1X+b_2Y, \tag{23b}$$

so that Eqs. (21) and (22) give:

$$3\left(\lambda\mu\left(1-\frac{1}{2}((b_1-1)X+(b_2-1)Y)^2\right)\right.$$
$$\left.(b_1\ddot{X}+b_2\ddot{Y})+2\mu\left(-\frac{1}{6}(X+Y)^3+X+Y\right)\right.$$
$$\left.-\frac{1}{6}(X+Y)^3+X+Y\right)$$
$$+3\lambda\mu(-b_1X-b_2Y+X+Y)\left(b_1\dot{X}+b_2\dot{Y}\right)^2$$
$$+(6\mu+2)(\ddot{X}+\ddot{Y})=0, \tag{24}$$

$$2\lambda\left(b_1\ddot{X}+b_2\ddot{Y}\right)+3\left(1-\frac{1}{2}((b_1-1)X\right.$$
$$\left.+(b_2-1)Y)^2\right)(\ddot{X}+\ddot{Y})-3(\ddot{X}+\ddot{Y})$$
$$(-b_1X-b_2Y+X+Y)$$
$$+3\left(-\frac{1}{6}(b_1X+b_2Y)^3+b_1X+b_2Y\right)=0, \tag{25}$$

For the case $\mu=1,\lambda=4/3$, the mode shape ratios are given by Eqs. (20a, 20b). Substituting these values into Eqs. (24) and (25), one has:

$$\left(-\frac{3X^2}{4}+\frac{15XY}{2}-\frac{75Y^2}{4}+14\right)\ddot{X}$$
$$+\left(\frac{3X^2}{4}-\frac{15XY}{2}+\frac{75Y^2}{4}+2\right)\ddot{Y}$$
$$-\frac{3X^3}{2}-\frac{9X^2Y}{2}-\frac{9XY^2}{2}-\frac{9X\dot{Y}^2}{2}$$
$$+9\dot{X}X\dot{Y},+\frac{45\dot{X}^2Y}{2}-45\dot{X}Y\dot{Y}-\frac{9\dot{X}^2X}{2}$$
$$+9X-\frac{3Y^3}{2}+\frac{45Y\dot{Y}^2}{2}+9Y=0, \tag{26}$$

$$\left(-\frac{3X^2}{8}+\frac{15XY}{4}-\frac{75Y^2}{8}+7\right)\ddot{X}$$
$$+\left(-\frac{3X^2}{8}+\frac{15XY}{4}-\frac{75Y^2}{8}-1\right)\ddot{Y}-\frac{27X^3}{16}$$
$$+\frac{81X^2Y}{16}-\frac{81XY^2}{16}+\frac{3X\dot{Y}^2}{2}+3\dot{X}X\dot{Y}$$
$$-\frac{15\dot{X}^2Y}{2}-15\dot{X}Y\dot{Y}+\frac{3\dot{X}^2X}{2}+\frac{9X}{2}+\frac{27Y^3}{16}$$
$$-\frac{15Y\dot{Y}^2}{2}-\frac{9Y}{2}=0. \tag{27}$$

The solutions for X and Y are assumed as series expansions that involve a small parameter ε :

$$X=\varepsilon X_0+\varepsilon^3X_1, \tag{28a}$$
$$Y=\varepsilon Y_0+\varepsilon^3Y_1. \tag{28b}$$

Their frequencies are assumed as the perturbations of the linear ones $\Omega_{10}=\omega_1=\frac{3\sqrt{14}}{14}$ and $\Omega_{20}=\omega_2=\frac{3\sqrt{2}}{2}$ (see Eqs. (19a, 19b)), i.e. as:

$$\Omega_1=\Omega_{10}+\varepsilon^2\Omega_{11}, \tag{29a}$$
$$\Omega_2=\Omega_{20}+\varepsilon^2\Omega_{21}, \tag{29b}$$

where the correction terms Ω_{11} and Ω_{21} need to be determined.

Thus, the velocities and acceleration terms in Eqs. (26) and (27) should be substituted by the terms:

$$\dot{X}=\Omega_1\left(\varepsilon\dot{X}_0+\varepsilon^3\dot{X}_1\right), \tag{30a}$$
$$\dot{Y}=\Omega_2\left(\varepsilon\dot{Y}_0+\varepsilon^3\dot{Y}_1\right), \tag{30b}$$

$$\ddot{X}=\Omega_1^2\left(\varepsilon\ddot{X}_0+\varepsilon^3\ddot{X}_1\right), \tag{31a}$$
$$\ddot{Y}=\Omega_2^2\left(\varepsilon\ddot{Y}_0+\varepsilon^3\ddot{Y}_1\right). \tag{31b}$$

Introducing Eqs. (28a, 28b)–(31a, 31b) into Eqs. (26) and (27), and collecting the terms next to the same powers of ε, one can derive

$$\varepsilon\left(\ddot{X}_0+X_0\right)+\frac{1}{336}\varepsilon^3\left(-3X_0^2\left(385Y_0-36\ddot{X}_0\right)\right.$$
$$\left.+3X_0\left(-360Y_0\ddot{X}_0-6\left(-10\sqrt{7}\dot{X}_0\dot{Y}_0\right.\right.\right.$$

$$+\dot{X}_0^2+7\dot{Y}_0^2\Big)+959Y_0^2\Big)+2700Y_0^2\ddot{X}_0+90\dot{X}_0^2Y_0$$
$$-900\sqrt{7}\dot{X}_0Y_0\dot{Y}_0+224\sqrt{14}\Omega_{11}\ddot{X}_0+336\ddot{X}_1$$
$$+35X_0^3+336X_1+35Y_0^3+630Y_0\dot{Y}_0^2\Big)=0, \tag{32}$$

$$\varepsilon\left(\ddot{Y}_0+Y_0\right)+\frac{1}{336}\varepsilon^3\Big(-3X_0^2\left(97Y_0-36\ddot{Y}_0\right)$$
$$+3X_0\Big(-6\Big(-2\sqrt{7}\dot{X}_0\dot{Y}_0+5\dot{X}_0^2+35\dot{Y}_0^2\Big)$$
$$-360Y_0\ddot{Y}_0+95Y_0^2\Big)+90Y_0$$
$$\Big(-2\sqrt{7}\dot{X}_0\dot{Y}_0+5\dot{X}_0^2+35\dot{Y}_0^2\Big)$$
$$+35X_0^3+112\Big(2\sqrt{2}\Omega_{21}\ddot{Y}_0+3\ddot{Y}_1+3Y_1\Big)$$
$$+2700Y_0^2\ddot{Y}_0-541Y_0^3\Big)=0. \tag{33}$$

The equations next to ε are the equations of motion of the harmonic oscillator with the natural frequency equal to unity:

$$\ddot{X}_0+X_0=0, \tag{34a}$$
$$\ddot{Y}_0+Y_0=0, \tag{34b}$$

and their solutions are:

$$X_0=A\cos(\tau), \tag{35a}$$
$$Y_0=B\cos(\tau). \tag{35b}$$

Equating to zero the coefficients next to ε^3 in Eqs. (32) and (33) and using Eqs. (35a, 35b), one derives

$$\ddot{X}_1+X_1=\frac{\left(-237A^3+45\left(4\sqrt{7}-3\right)A^2B+A\left(-45\left(20\sqrt{7}-9\right)B^2-896\sqrt{14}\Omega_{11}\right)+735B^3\right)}{1344}\cos(\tau)$$
$$+\frac{\left(-55A^3-15\left(11+12\sqrt{7}\right)A^2B+3\left(101+300\sqrt{7}\right)AB^2-595B^3\right)}{1344}\cos(3\tau), \tag{36}$$

$$\ddot{Y}_1+Y_1=\frac{\left(15A^3+9\left(4\sqrt{7}-83\right)A^2B-45\left(4\sqrt{7}-77\right)AB^2-7B\left(939B^2+128\sqrt{2}\Omega_{21}\right)\right)}{1344}\cos(\tau)$$
$$+\frac{\left(125A^3-3\left(283+12\sqrt{7}\right)A^2B+15\left(133+12\sqrt{7}\right)AB^2-6391B^3\right)}{1344}\cos(3\tau). \tag{37}$$

The coefficients next to $\cos(\tau)$ represent the so-called secular terms and must be equal to zero, which yields:

$$-237A^3+45(4\sqrt{7}-3)A^2B+A(-45(20\sqrt{7}-9)B^2$$
$$-896\sqrt{14}\Omega_{11})+735B^3=0, \tag{38}$$
$$15A^3+9(4\sqrt{7}-83)A^2B-45(4\sqrt{7}-77)AB^2$$
$$-7B(939B^2+128\sqrt{2}\Omega_{21})=0. \tag{39}$$

These two equations lead to the correction terms for the frequencies of motion in Eqs. (29a, 29b), which are given by:

$$\Omega_{11}=\frac{3(-79A^3+15(4\sqrt{7}-3)A^2B+15(9-20\sqrt{7})AB^2+245B^3)}{896\sqrt{14}A}$$
$$=-0.071A^2+\frac{0.219B^3}{A}+0.102AB-0.589B^2, \tag{40}$$
$$\Omega_{21}=\frac{3(5A^3+3(4\sqrt{7}-83)A^2B+15(77-4\sqrt{7})AB^2-2191B^3)}{896\sqrt{2}B}$$
$$=\frac{0.012A^3}{B}-0.514A^2+2.359AB-5.187B^2. \tag{41}$$

It is seen that the influence of the initial amplitudes on the frequency correction terms is of a quadratic power form. The values of the coefficients in Eqs. (40) and (41) in front of B^2 and A^2 imply that the former has the stronger influence on them than the latter.

Thus, the solutions sought are:

$$X=A\cos\left(\left(\Omega_{10}+\varepsilon^2\Omega_{11}\right)\tau\right), \tag{42a}$$
$$Y=B\cos\left(\left(\Omega_{20}+\varepsilon^2\Omega_{21}\right)\tau\right). \tag{42b}$$

The accuracy of the solutions given by Eqs. (42a, 42b), (29a, 29b), (40), (41) is checked by comparing it with numerical solution of the exact equations of motion. These comparisons are shown in Fig. 8 for different nonzero initial amplitudes and zero initial velocities. It is seen that the agreement between these two types of solutions is reasonably good.

Now, based on Eqs. (23a, 23b), one can go back to the original generalized coordinates ($A_1=A+B$, $A_2=1.5A-1.5B$) and use $\Omega_1=\Omega_2$ to obtain the combinations of the initial amplitudes A_1 and A_2 that would result in NNM1 and NNM2. These solutions

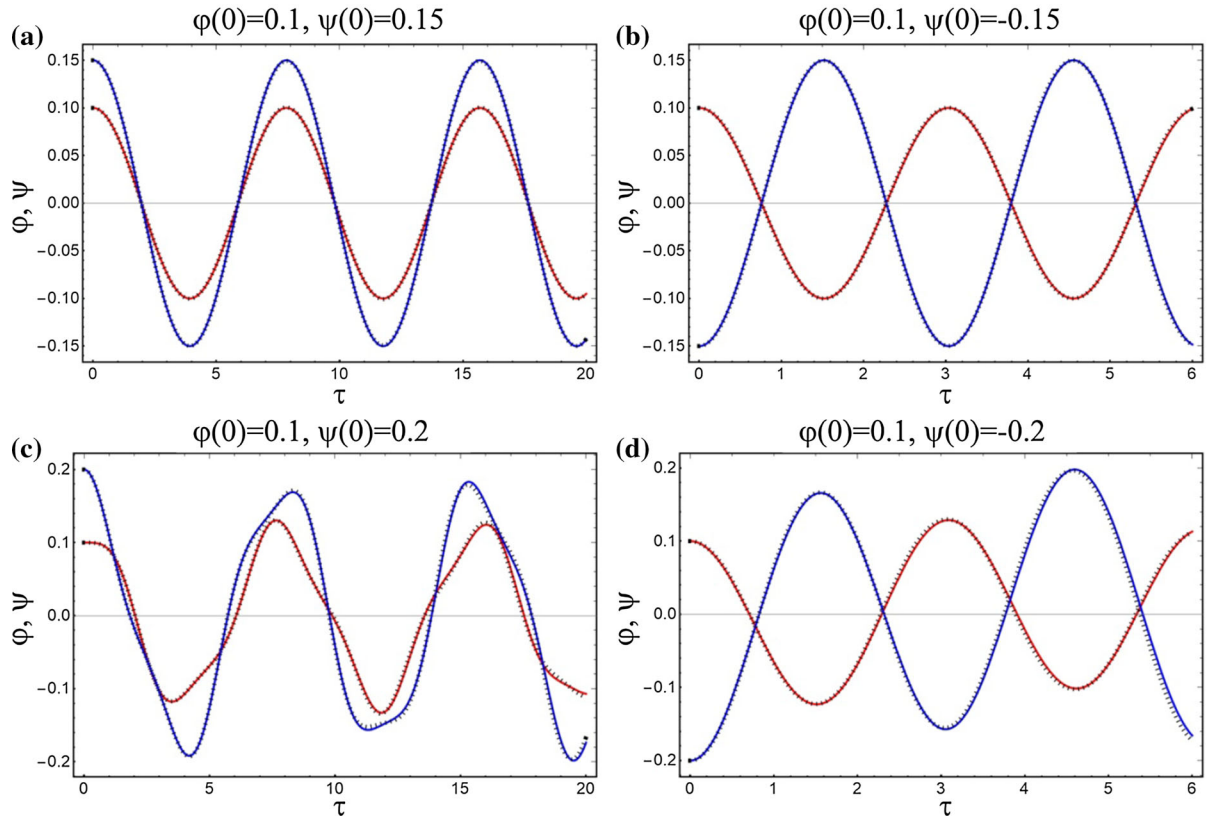

Fig. 8 Case $\mu = 1, \lambda = 4/3$: comparison of the approximate analytical solutions (solid lines) given by Eqs. (42a, 42b), (29a, 29b), (40), (41) with the numerical solutions (doted lines) of the exact equations of motion for different nonzero initial amplitudes and zero initial velocities indicated above each figure

are plotted in Fig. 9 as blue circles, together with the solutions for the linear case (green lines) and the solutions for the exact equations of motion (solid lines). The approximate solutions are found to agree reasonably well with the numerical ones until the value $A_1 = 0.3$, approximately.

3.3 Approximate solutions by harmonic balancing

The approximate solution obtained in the previous section has a limited range of accuracy, and, thus, the aim of this section is to look for the solution that will be accurate for larger values of the initial amplitudes. To that end, harmonic balancing is to be used.

By introducing the approximations: $\sin\varphi \approx \varphi - \frac{\varphi^3}{6}$, $\sin\psi \approx \psi - \frac{\psi^3}{6}$, $\cos\varphi \approx 1 - \frac{\varphi^2}{2}$, $\cos\psi \approx 1 - \frac{\psi^2}{2}$, into the exact equations of motion given by Eqs. (6) and (7),

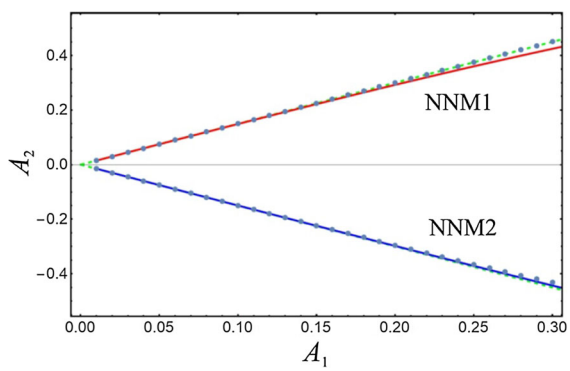

Fig. 9 Case $\mu = 1, \lambda = 4/3$: combinations of initial amplitudes yielding vibrations in normal modes. Green dotes—solutions for the linear system; red solid line—solutions for A_1 (NNM1); and blue solid line—solutions for A_2(NNM2); blue circles—analytical approximate solution by the Lindstedt–Poincaré method. (Color figure online)

the following approximated differential equations are obtained:

$$
\begin{aligned}
&6\mu\ddot{\varphi}+2\ddot{\varphi}+3\lambda\mu\left(1-\frac{\varphi^2}{2}\right)\left(1-\frac{\psi^2}{2}\right)\ddot{\psi}\\
&+3\lambda\mu\left(\varphi-\frac{\varphi^3}{6}\right)\left(\psi-\frac{\psi^3}{6}\right)\ddot{\psi}\\
&+3\left(\varphi-\frac{\varphi^3}{6}\right)+6\mu\left(\varphi-\frac{\varphi^3}{6}\right)\\
&+3\lambda\mu\left(\varphi-\frac{\varphi^3}{6}\right)\left(1-\frac{\psi^2}{2}\right)\dot{\psi}^2\\
&-3\lambda\mu\left(1-\frac{\varphi^2}{2}\right)\left(\psi-\frac{\psi^3}{6}\right)\dot{\psi}^2=0, \qquad (43)\\
&3\left(1-\frac{\varphi^2}{2}\right)\left(1-\frac{\psi^2}{2}\right)\ddot{\varphi}+3\left(\varphi-\frac{\varphi^3}{6}\right)\left(\psi-\frac{\psi^3}{6}\right)\ddot{\varphi}\\
&+2\lambda\ddot{\psi}+3\left(\psi-\frac{\psi^3}{6}\right)-3\left(\varphi-\frac{\varphi^3}{6}\right)\left(1-\frac{\psi^2}{2}\right)\dot{\varphi}^2\\
&+3\left(1-\frac{\varphi^2}{2}\right)\left(\psi-\frac{\psi^3}{6}\right)\dot{\varphi}^2=0. \qquad (44)
\end{aligned}
$$

Given the existence of cubic nonlinearity, the solutions for motion are taken in the form that involves the first and second harmonic:

$$\varphi=\varepsilon\bar{A}_1\cos(\omega\tau)+\varepsilon^2\bar{B}_1\cos(3\omega\tau), \qquad (45a)$$

$$\psi=\varepsilon\bar{A}_2\cos(\omega\tau)+\varepsilon^2\bar{B}_2\cos(3\omega\tau). \qquad (45b)$$

The initial velocities are assumed to be zero $\dot{\varphi}(0)=0, \dot{\psi}(0)=0$, while the initial amplitudes A_1 and A_2 satisfy:

$$\varepsilon\bar{A}_1+\varepsilon^2\bar{B}_1=A_1=\varphi(0), \qquad (46a)$$

$$\varepsilon\bar{A}_2+\varepsilon^2\bar{B}_2=A_2=\psi(0). \qquad (46b)$$

Substituting Eqs. (45a, 45b) and its first and second derivatives into Eqs. (43) and (44), grouping the terms next to $\cos(\omega\tau)$ and then next to the same power of ε, one obtains:

$$
\begin{aligned}
&-\frac{3}{8}(4\lambda\mu\bar{A}_2^2\bar{B}_1\omega^2-2\lambda\mu\bar{A}_1\bar{A}_2\bar{B}_1\omega^2\\
&-9\lambda\mu\bar{A}_1^2\bar{B}_2\omega^2-\lambda\mu\bar{A}_2^2\bar{B}_2\omega^2+8\lambda\mu\bar{A}_1\bar{A}_2\bar{B}_2\omega^2\\
&+2\mu\bar{A}_1^2\bar{B}_1+\bar{A}_1^2\bar{B}_1)\varepsilon^4-\frac{3}{8}\left(2\mu\bar{A}_1^3+\bar{A}_1^3\right.\\
&\left.-3\lambda\mu\omega^2\bar{A}_2\bar{A}_1^2+4\lambda\mu\omega^2\bar{A}_2^2\bar{A}_1-\lambda\mu\omega^2\bar{A}_2^3\right)\varepsilon^3\\
&+(-6\mu\bar{A}_1\omega^2-2\bar{A}_1\omega^2-3\lambda\mu\bar{A}_2\omega^2\\
&+6\mu\bar{A}_1+3\bar{A}_1)\varepsilon=0, \qquad (47)\\
&\frac{3}{8}\left(\bar{A}_1^2\bar{B}_1\omega^2+9\bar{A}_2^2\bar{B}_1\omega^2-8\bar{A}_1\bar{A}_2\bar{B}_1\omega^2\right.\\
&\left.-4\bar{A}_1^2\bar{B}_2\omega^2+2\bar{A}_1\bar{A}_2\bar{B}_2\omega^2-\bar{A}_2^2\bar{B}_2\right)\varepsilon^4\\
&+\frac{3}{8}(\omega^2\bar{A}_1^3-4\omega^2\bar{A}_2\bar{A}_1^2+3\omega^2\bar{A}_2^2\bar{A}_1-\bar{A}_2^3)\varepsilon^3\\
&+\left(-3\bar{A}_1\omega^2-2\lambda\bar{A}_2\omega^2+3\bar{A}_2\right)\varepsilon=0. \qquad (48)
\end{aligned}
$$

Repeating the same procedure for the terms next to $\cos(3\omega\tau)$, it follows:

$$
\begin{aligned}
&-\frac{3}{4}\left(-2\lambda\mu\bar{A}_1\bar{A}_2\bar{B}_1\omega^2-9\lambda\mu\bar{A}_1^2\bar{B}_2\omega^2\right.\\
&-9\lambda\mu\bar{A}_2^2\bar{B}_2\omega^2+20\lambda\mu\bar{A}_1\bar{A}_2\bar{B}_2\omega^2\\
&\left.+2\mu\bar{A}_1^2\bar{B}_1+\bar{A}_1^2\bar{B}_1\right)\varepsilon^4+\frac{1}{8}\left(-2\mu\bar{A}_1^3-\bar{A}_1^3\right.\\
&\left.+3\lambda\mu\omega^2\bar{A}_2\bar{A}_1^2-12\lambda\mu\omega^2\bar{A}_2^2\bar{A}_1+9\lambda\mu\omega^2\bar{A}_2^3\right)\varepsilon^3\\
&+(-54\mu\bar{B}_1\omega^2-18\bar{B}_1\omega^2-27\lambda\mu\bar{B}_2\omega^2\\
&+6\mu\bar{B}_1+3\bar{B}_1)\varepsilon^2=0, \qquad (49)\\
&\frac{3}{4}\left(9\bar{A}_1^2\bar{B}_1\omega^2+9\bar{A}_2^2\bar{B}_1\omega^2-20\bar{A}_1\bar{A}_2\bar{B}_1\omega^2\right.\\
&\left.+2\bar{A}_1\bar{A}_2\bar{B}_2\omega^2-\bar{A}_2^2\bar{B}_2\right)\varepsilon^4\\
&+\frac{1}{8}(9\omega^2\bar{A}_1^3-12\omega^2\bar{A}_2\bar{A}_1^2+3\omega^2\bar{A}_2^2\bar{A}_1-\bar{A}_2^3)\varepsilon^3\\
&+\left(-27\bar{B}_1\omega^2-18\lambda\bar{B}_2\omega^2+3\bar{B}_2\right)\varepsilon^2=0. \qquad (50)
\end{aligned}
$$

In order to calculate five unknown quantities: $\bar{A}_1, \bar{B}_1, \bar{A}_2, \bar{B}_2, \omega$, one should fix $A_1=\varphi(0)$ and then solve numerically the system of five equations (47)–(50) and (46a). The accuracy of the approximate solutions obtained is compared with the numerical solutions of the exact equations of motion. These comparisons are shown in Fig. 10 for different nonzero initial amplitudes and zero initial velocities. The agreement between these two types of solutions is very good.

The approximate solutions for normal modes, $A_2=\psi(0)=\varepsilon\bar{A}_2+\varepsilon^2\bar{B}_2$, are plotted in Fig. 11 as a function of the fixed value $A_1=\varphi(0)=\varepsilon\bar{A}_1+\varepsilon^2\bar{B}_1$ as the blue circles. The solutions for the linear case (green lines) and the solutions for the exact equations of motion (solid lines) are compared. The approximate solutions are found to agree reasonably well with the numerical ones until the value A_1 slightly larger than 0.7, which is considerably larger value than the one achieved in the previous section by the Lindstedt–Poincaré method. This is also shown in Fig. 12, illustrating the comparison of the analytical results obtained

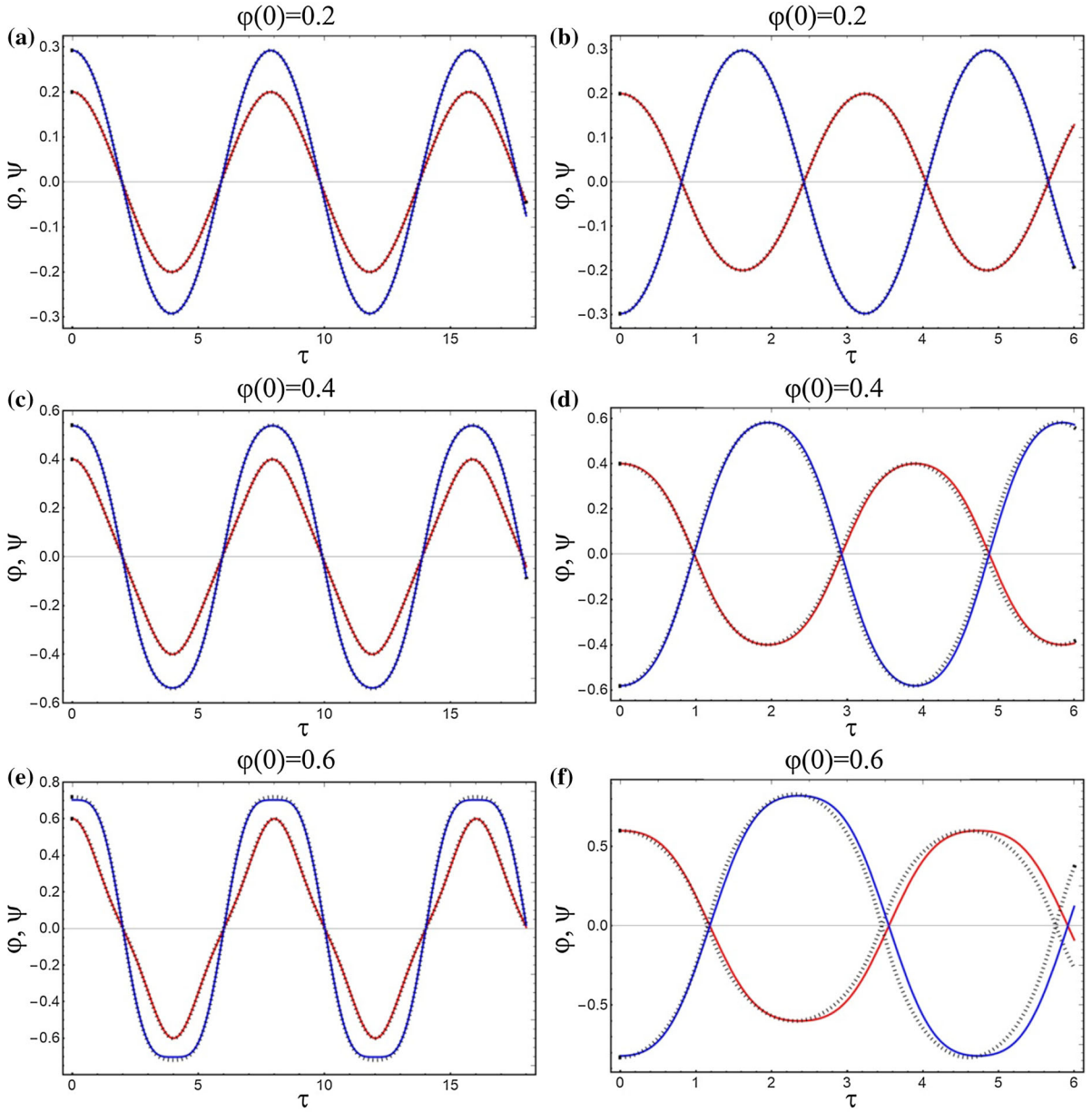

Fig. 10 Case $\mu = 1, \lambda = 4/3$: comparison of the approximate analytical solutions (solid lines) obtained by harmonic balancing with the numerical solutions (doted lines) of the exact equations of motion for different nonzero initial amplitudes and zero initial velocities indicated above each figure

by both approaches. However, the solution obtained by the Lindstedt–Poincaré method gives the explicit expressions for the influence of the initial amplitudes on the frequencies, unlike harmonic balancing whose solutions are implicit and semi-analytical.

The results obtained by harmonic balancing are also added to Fig. 2c to the energy level diagram as the red circles connected by the thick black line, to emphasized the combinations of the initial amplitudes that yield the desirable level of the initial energy, which has been the main task of this work.

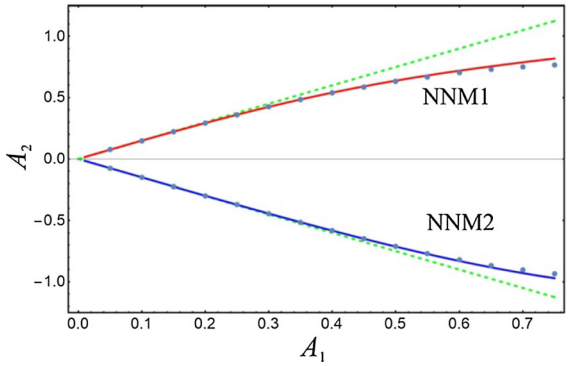

Fig. 11 Case $\mu = 1, \lambda = 4/3$: combinations of initial amplitudes yielding vibrations in normal modes. Green dotes—solutions for the linear system; red solid line—solutions for A_1 (NNM1); and blue solid line—solutions for A_2(NNM2); blue circles—analytical approximate solution by harmonic balancing. (Color figure online)

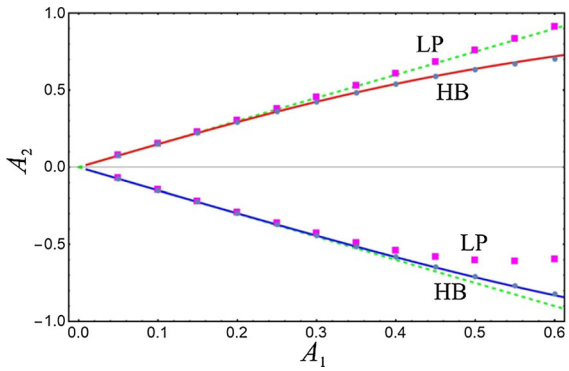

Fig. 12 Case $\mu = 1, \lambda = 4/3$: combinations of initial amplitudes yielding vibrations in normal modes. Green dotes—solutions for the linear system; red solid line—solutions for A_1 (NNM1); and blue solid line—solutions for A_2(NNM2); blue circles—analytical approximate solution by harmonic balancing; magenta squares—analytical approximate solution by the Lindstedt–Poincaré method. (Color figure online)

4 Conclusions

A planar double pendulum moving in a vertical plane, consisting of two uniform massive unequal or equal rods, has been considered in this work. The influence of energy levels on the fixed points (centres and saddles) and the type of trajectories have been determined (closed trajectories, separatrices and the trajectories corresponding to spinning). Then, the focus has been set on the determined domain of low levels of energy and the linear and nonlinear normal modes that occur then. First, the case of small (linear) oscillations has been examined. The mode shape ratios and the associated natural frequencies have been found for an in-phase mode (Mode 1) and an out-of-phase mode (Mode 2). Then, the case of larger-amplitude (nonlinear) oscillations has been investigated via numerical and approximate analytical approaches, focusing on the appearance of in-phase nonlinear normal mode NNM1 (analogous to Mode 1 in the linear system) and an out-of-phase nonlinear normal mode NNM2 (analogous to Mode 2 in the linear system). The combinations of the initial amplitudes of the pendula for which they occur have been determined. The corresponding angular frequencies have also been obtained as the functions of the initial amplitudes and compared with the linear case. It has been concluded that as the value of the initial amplitude of the upper pendulum A_1 increases, the absolute values of the initial amplitude of the lower pendulum A_2 decrease for both NNM1 and NNM2. Besides this, as the initial amplitudes increase, the frequency of NNM1 decreases from the value corresponding to the frequency of the linear Mode 1. By decreasing the absolute values of the initial amplitudes, the frequency of NNM2 increases until the value of the frequency of the linear Mode 2. These conclusions have been obtained based on two approximate analytical approaches that have been adjusted for this purpose: the Lindstedt–Poincaré method and harmonic balancing, and they have been confirmed numerically. Harmonic balancing is accurate for larger initial amplitudes, but does not give explicit expressions for the influence of the initial amplitudes on the angular frequencies, while the Lindstedt–Poincaré method is accurate for smaller initial amplitudes, but does give explicit power-form expressions for the influence of the initial amplitudes on the angular frequencies.

Acknowledgements The authors acknowledge support of the Ministry of Education and Science of Serbia, Grant III41007.

Compliance with ethical standards

Conflict of interest The authors declare that they have no conflict of interest.

References

1. Nayfeh, A.H., Mook, D.T.: Nonlinear Oscillations. Wiley, New York (1979)
2. Kovacic, I., Rand, R.H.: About a class of nonlinear oscillators with amplitude-independent frequency. Nonlinear Dyn. **74**, 455–465 (2013)

3. Poschel, J.: A lecture on the classical KAM theorem. Proc. Symp. Pure Math. **69**, 707–732 (2001)
4. Richter, P.H., Scholz, H.J.: Chaos in classical mechanics: the double pendulum. In: Schuster, P. (ed.) Stochastic Phenomena and Chaotic Behaviour in Complex Systems. Springer Series in Synergetics, vol. 21, pp. 86–97. Springer, Berlin (1984)
5. Shinbrot, T., Grebogi, C., Wisdom, J., Yorke, J.A.: Chaos in a double pendulum. Am. J. Phys. **60**, 491–499 (1992)
6. Levien, R.B., Tan, S.M.: Double pendulum: an experiment in chaos. Am. J. Phys. **61**, 1038–1044 (1993)
7. Stachowiak, T., Okada, T.: A numerical analysis of chaos in the double pendulum. Chaos Solitons Fract. **29**, 417–422 (2006)
8. Rafat, M.Z., Wheatland, M.S., Bedding, T.R.: Dynamics of a double pendulum with distributed mass. Am. J. Phys. **77**, 216–223 (2009)
9. Jyotirmoy, R., Mallik, A.K., Bhattacharjee, J.K.: Role of initial conditions in the dynamics of a double pendulum at low energies. Nonlinear Dyn. **73**, 993–1004 (2013)
10. Kovacic, I., Radomirovic, D.: Mechanical Vibrations: Fundamentals with Solved Examples. Willey, London (2017)
11. Rosenberg, R.: The normal modes of nonlinear n-degree-of-freedom systems. J. Appl. Mech. **2**, 7–14 (1962)